

## Nonlocal damage modelling using the element-free Galerkin method in the frame of finite strains

Xiaofei Pan<sup>1</sup>, Huang Yuan<sup>1,a</sup>

<sup>1</sup>Department of Mech. Eng., University of Wuppertal, Germany

<sup>a</sup>h.yuan@uni-wuppertal.de

**Keywords:** Meshless method; element-free Galerkin; nonlocal damage; gradient plasticity; size effects.

**Abstract.** Computational analysis of damage failure is of great importance in predicting assessment of structure integrity. Numerical modeling of ductile material damage using finite element methods often suffers from convergence problems of numerical iteration, especially, when working with a complex constitutive model as gradient plasticity and nonlocal damage models. Due to large strains in damaging elements the computation may result in non-convergence. For the higher order gradient plasticity the element formulation is often necessary, which causes additional difficulties in implementation and computations. In recent years meshless methods have been developed as an alternative for the finite element method (FEM) and can overcome some known shortcomings of the latter. One major advantage of the meshless methods is in continuous differentiation of the strain tensor for cases with finite strains. Complex constitutive models, such as gradient plasticity nonlocal damage models, are easy to be applied in meshless methods. In the present paper we have developed and implemented an algorithm of element-free Galerkin (EFG) methods for strain-gradient based nonlocal damage models and used it to simulate ductile material damage. The method provides a reliable and robust method for material failure with large damage zones. With the help of the meshless method material failure of specimens as well as the size effect are predicted accurately.

### 1. Introduction

Most engineering material displays significant dependence on the absolute size of the specimen, so called size effects. It has been recognized that the size effect is related to micro-structural characteristic in the material and variety of models incorporating material length scale has been proposed [12]. In ductile materials failure is characterized by micro-void nucleation, growth and coalescence mechanism as introduced by the GTN model [3,4], since it is not derived from purely heuristic arguments but from micro-mechanical analysis. In order to catch size effects, several nonlocal forms of the GTN models have been proposed [2, 5-7]. Due to the high order differentiation of nonlocal treatments, the conventional finite element technique may become inapplicable. A robust computational algorithm is essential for the validation and application of such a complex constitutive model. In finite element methods, the nodes are attached with the elements. It is difficult to construct high order continuous element which is often necessary when the high order gradient plasticity theory is applied. Furthermore when material is deformed largely due to damaging loading, the meshes will be distorted which will result in non-convergence, the decreasing of the accuracy and even the terminal of computation.

In the last years, meshless methods have been developed rapidly [8-12]. Differently from the FEM, meshless methods construct shape function with a series of nodes which is not related to meshes. Among meshless methods, element-free Galerkin method (EFG) is one of the most famous ones. One of advantages of EFG is that it is possible to model arbitrary growth of cracks without re-meshing or adaptive refinement at the crack tip is easily accomplished. With adequate refinement, stress intensity factors can be computed accurately. EFG method has been applied for elastic-plastic

fracture analysis [9,10]. All of the former EFG cracks analyses are with local models, and no size effects are considered [14]. Another advantage of EFG is that it has ability to incorporate higher-order gradients in a straightforward manner, so complex constitutive models such as gradient plasticity or elasticity models are very easy to be applied [12,13]. In the presenting paper, we are applying nonlocal damage model suggested in [7] with element-free Galerkin method to analyze the damage procedure and size effects in a German reactor steel.

## 2. Nonlocal damage model based on the gradient plasticity

It is known that in conventional solid mechanics, the stress state is determined by the deformation history at the single material point, the local assumption. The conventional solid mechanics is quite sufficient for most applications, but there are some experimental evidences indicating that under certain circumstances the material micro-structure must be taken into account in a suitable way. Recently, the material modeling including micro-structure characteristics has been extensively discussed [1, 2, 5-7]. As suggested by Aifantis [1], the flow stress depends on both plastic strain and its gradients as

$$Y = \sigma_y(\bar{\epsilon}^p) + \psi\left(\left|\nabla\bar{\epsilon}^p\right|, \Delta\bar{\epsilon}^p, \dots\right), \quad (1)$$

where  $\sigma_y(\bar{\epsilon}^p)$  denotes the yield stress measured in uniaxial tensile tests and  $\bar{\epsilon}^p$  is the equivalent plastic strain.  $\psi$  is a function which introduces the intrinsic material length scale characterizing micro-structures via the strain gradients. In the present paper the function suggested by Aifantis as

$$Y(\bar{\epsilon}^p, \Delta\bar{\epsilon}^p) = \sigma_y(\bar{\epsilon}^p) + g\Delta\bar{\epsilon}^p, \quad (2)$$

where  $g$  is a positive coefficient with the dimension of force and assumed as  $g = \sigma_0 l^2$  with  $\sigma_0$  as the initial yield stress and  $l$  as an intrinsic material length scale characterizing micro-structures of the material. Through introducing the plasticity theory based on the strain-gradient into the GTN model [3,4], the yield function of the micro-mechanical damage model (GTN model) can be written as

$$\Phi\left(\sigma_{ij}, \bar{\epsilon}^p, \Delta\bar{\epsilon}^p, f^*\right) = \left(\frac{q}{Y(\bar{\epsilon}^p, \Delta\bar{\epsilon}^p)}\right)^2 + 2q_1 f^* \cosh\left(\frac{3q_2 p}{2Y(\bar{\epsilon}^p, \Delta\bar{\epsilon}^p)}\right) - \left(1 + q_1^2 f^{*2}\right), \quad (3)$$

where the constants  $q_1$  and  $q_2$  are introduced [4] to bring predictions of the model into closer agreement with full numerical analysis.  $q$  is the Mises stress,  $p$  the hydrostatic stress, and  $f^*$  the effective porosity as defined by Tvergaard [4].

Due to the gradient-dependent yield stress the strain localization is avoided as shown in [7]. The gradient of the second order in the yield surface the FEM implementation requires  $C^1$  element formulation [7] which causes significant convergence problems especially in failing elements. In the implicit method of solving large-deformation problems, the discretized equilibrium equations result in a set of nonlinear equations for the nodal unknown at the end of the increment. In this paper, element free Galerkin method is implemented as a user's subroutine in the ABAQUS code which uses Newton's method [15].

## 3. Element-free Galerkin algorithm

The moving least-square approximation is one of the most common meshless methods introduced a spatial discretization in the numerical solution of boundary value problems. In the method, only a set of nodes and a boundary description are needed to develop the Galerkin equations. The interpolants are polynomials that are fit to the nodal values by a least square approximation. The approximation was not recognized as moving least squares (MLS), referred to as *diffuse elements*, and the method was viewed as a generalization of the finite element method (FEM). In MLS, the interpolation of the function  $u(\mathbf{X})$  is defined in the domain  $\Omega$  as

$$u^h(\mathbf{X}) = \sum_{i=1}^m p_i(\mathbf{X}) a_i(\mathbf{X}) = \mathbf{p}^T(\mathbf{X}) \mathbf{a}(\mathbf{X}), \quad (4)$$

where  $\mathbf{X}$  denotes the material coordinate in the initial configuration,  $m$  is the number of terms in the basis,  $\mathbf{p}(\mathbf{X})$  is the monomial basis function, and  $\mathbf{a}(\mathbf{X})$  is the coefficients which are functions of  $\mathbf{X}$ . Examples of commonly used are linear basis and the quadratic basis. The coefficients  $\mathbf{a}(\mathbf{X})$  are obtained by performing a weighted least square fit for the local approximation, which is obtained by minimizing the difference between the local approximation and the function, with

$$\begin{aligned} J &= \sum_I w(\mathbf{X} - \mathbf{X}_I) \left[ u^h(\mathbf{X}, \mathbf{X}_I) - u(\mathbf{X}_I) \right]^2 \\ &= \sum_I w(\mathbf{X} - \mathbf{X}_I) \left[ \sum_i p_i(\mathbf{X}_I) a_i(\mathbf{X}) - u(\mathbf{X}_I) \right]^2 \end{aligned} \quad (5)$$

The approximation  $u^h(\mathbf{X})$  can be expressed in the form of shape functions,  $\phi_i(\mathbf{X})$ , and nodal values,  $u_i$ , as

$$u^h(\mathbf{X}) = \sum_I \phi_I(\mathbf{X}) u_I. \quad (6)$$

The consistency of order  $k$  of the MLS approximation can be satisfied if the basis is complete in the polynomials of order  $k$ . In fact, any function, which appears in the basis, can be reproduced exactly by a MLS approximation.

In this paper, the updated Lagrangian formulation is used, and the derivation of variables from the coordinates in the spatial configuration is needed. In the present work the gradients of the plastic strain are calculated directly from the interpolation. The governing equation for the element-free Galerkin method can be built from

$$\int \sigma_{ij} \delta u_{i,j} dV = 0, \quad (7)$$

where  $\delta u_i$  is the virtual incremental displacement. In the governing equations all variables are defined in the current configuration. To solve the non-linear differential integro-equation, the Newton method is used [13].

In EFG the integration is often performed with help of background cells. In our program, the initial integration points for EFG are composed by all Gauss integration points of the background elements which can be generated from the existing commercial FEM software. In the later time steps, the integration points move with the materials.

#### 4. Implementation of the EFG algorithm into ABAQUS

ABAQUS provides a user interface, UEL, to implement user-defined elements in which both stiffness matrices and nodal force vectors have to be defined. In UEL, the nodes constructing the elements should be defined. For FEM, elements are constructed by meshes, while in EFG there does not exist meshes but support domains. In our EFG implementation, we treat the support domains of integration points as elements. The support domain of a point  $\mathbf{x}$  is constructed by the nodes, of which the definition domain can support, also those nodes are required to define the corresponding user-defined element. In this sense the user element of the EFG contain generally much more nodes than in the conventional FEM element.

When we use user-defined elements, the number of nodes constructing elements of one type should be fixed, while in meshless algorithm the number of nodes in support domains is varying. It is impossible to define too many user-defined element types, so in our implementation, when defining the user-define element type, we set an upper bound as the number of required nodes, also the elements are constructed with the corresponding number of nodes which is often beyond the practice, while in actual implementation only those nodes in support domain are used.

Note that the treatment of essential boundaries in meshless methods is different from that in FEM. Generally speaking, the meshless shape function has no Dirac function property, and the boundary displacement cannot be dealt with as simply as in FEM. In our program the penalty method is used. To do that the nodes on the essential boundaries are also regarded as the user-defined elements just like Gauss integration point. So in the meshless algorithm for UEL, the user-defined elements are composed two parts. The first ones are from the Gauss points on the background meshes, in which the element stiffness matrices should be defined. The other ones are from the boundary nodes, in which the penalty matrices and displacement vectors are calculated. For every element, the stiffness matrix or penalty matrix is added to the matrix 'AMATRX' defined in UEL which contains the contribution of this element to the Jacobian (stiffness) or is other matrix of the overall system of equations, and the displacement vector is added to the vector 'RHS' which is also defined in UEL and contains the contributions of this element to the right-hand-side vectors of the overall system of equations.

### 5. Computational results

Computations of the present work are based on the German reactor pressure vessel steel, 20MnMn55 [7]. Experimental data reported in the present paper were determined within a European research project [7]. The material parameters fit from the experimental tests are as following: Young's modulus  $E=220$  GPa, initial yield stress  $\sigma_0=445$ MPa, and the hardening curve is expressed as

$$\int \sigma_y = \begin{cases} \sigma_0 & \bar{\epsilon}^p \leq 0.01, \\ 898(\bar{\epsilon}^p - 0.0067)^{1/8.13} & \bar{\epsilon}^p > 0.01. \end{cases} \quad (7)$$

To identify the material length parameter in the present nonlocal damage is a special task. From discussions in [7] the material length is related to plastic deformation and describes localized plastic deformation. The material length can be determined based on numerical experiments. Summarizing the simulations of different specimens we find that the material length should be between 0.2mm and 0.3 mm.

#### 5.1 Analysis of uniaxial tension specimens

The uniaxial tension tests are performed at room temperature. Different strain rate from  $10^{-5}$  to  $10^{-3}$  are examined which shows that the effects of the strain rates are insignificant. To study effects of the specimen size on tensile strength, a series of uniaxial tests has been performed. The specimen diameters are 3, 9 and 30 mm named R1, R2 and R3, respectively. The geometry of all specimens is shown in Fig. 1. All specimens discussed in the present paper are free of residual stress at the initial state and tested at the room temperature. Before material damage becomes significant in the tension process, deformations in the specimens are homogeneous and the stress is a monotonic increasing function of the strain, the measured stress vs. strain is independent of the specimen size. Furthermore the specimen begins to neck where the material is relatively weaker due to e.g. heterogeneity than elsewhere. As soon as the specimen necking starts,

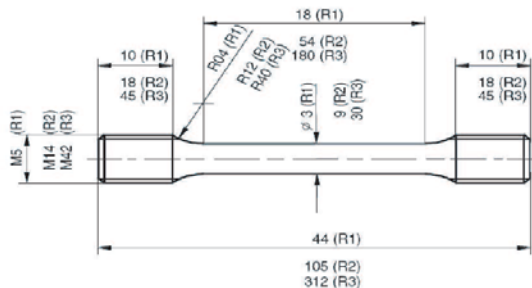


Figure 1: Geometry of the uniaxial tension specimens. Three different sizes are considered [7].

the traction decreases and the stress state around the necking becomes triaxial. The necking and triaxial stress state let strain growth localize in a small process.

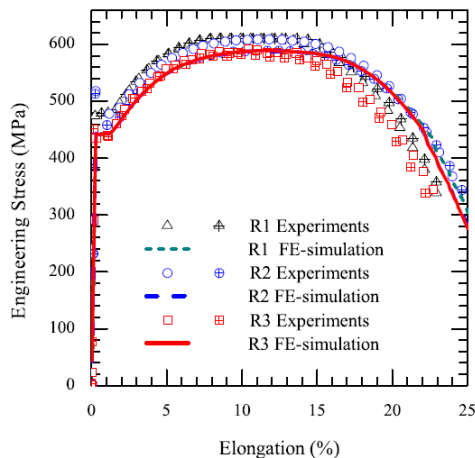
The computational results of engineering stress vs. elongation are compared with that of experiments. In Fig. 2, the computational results are plotted as curves while the experimental ones are plotted as symbols, and the former agree well with the latter. The uniaxial tension records do not show obvious influence of the specimen sizes. It can be seen from the picture that the results of the smallest specimen R1 is only very slightly different from that of the other cases which supports that the prediction of the gradient plasticity manifesting the size effect correlates with the plastic strain gradients.

Fig. 3 shows the results of elongation vs. necking which is defined as  $\Delta R/R_0$  and denotes the radius variation ratio, where  $R_0$  is the initial radius in the middle specimen and  $\Delta R$  is the corresponding variation. The computations agree well with experiments [7]. Before material damage becomes significant the necking is a monotonic increasing function of the elongation and the ratio is about 2. Actually, in this case the deformation is homogeneous and the volumes of specimens are approximately invariable compared with the plastic deformation. With damage growth the necking becomes much acuter.

### 5.2 Analysis of notched specimens

The numerical and experimental results of the uniaxial tension specimens confirm that the size effect in material deformations and failure are not related to the strain amplitude. In this section, a series of notched tension specimens is tested under the same condition as the uniaxial specimens. Three specimen geometries are considered termed as T1, T2 and T3, as plotted in Fig. 4. The scaling factors are 1, 3 and 10, respectively.

In Fig. 5 both computational and experimental results of engineering stress vs. elongation are summarized. The scatters denote the experimental results and the curves denote the numerical ones and they agree well. The engineering stress is defined as the tensile force per unit area in the middle of the undeformed specimens. Fig. 5 shows significant influence of specimen sizes. The smaller specimen shows a smoother stress variation, and the engineering stress of specimen T1 is significantly larger than that of specimen T2 and T3 when the elongation is about larger than 4%



**Figure 2:** Comparison between the experimental and computational results of engineering stress vs. elongation for smooth tensile specimens R1, R2 and R3.

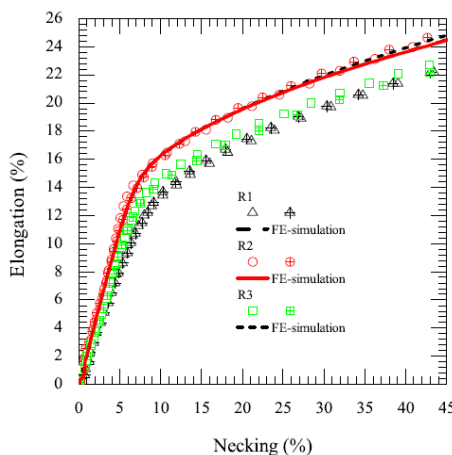


**Figure 3:** Comparison between the experimental and computational results of necking vs. elongation for smooth tensile specimens R1, R2 and R3.

which is to say that smaller specimen can bear larger stress. T2 and T3 do not display obviously influence of specimen size.

Engineering stress vs. necking of the notched specimens is displayed in Fig. 6. The computational results agree not very well for low loading levels, although they all show significant size effects. The experimental results show that the specimens neck quickly between the points of about 1.0% and 4.0% elongation.

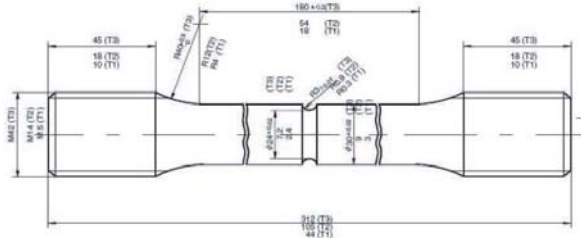


Figure 4: Geometry of notched specimens. Three sizes are considered.

illustrated as following: the damage firstly takes place in the in the notched area when the specimens are tensed, which can be seen from Fig.7. The damage area near the notched section becomes unaltered after it reaches at certain value. Finally, the damage takes place from the center of the specimens just like the smooth ones. During the actual measure procedure, the measure tool could intrude the damage area near the notched section which seems that the measured radius of specimens becomes smaller. This result has been observed in other analysis [7].

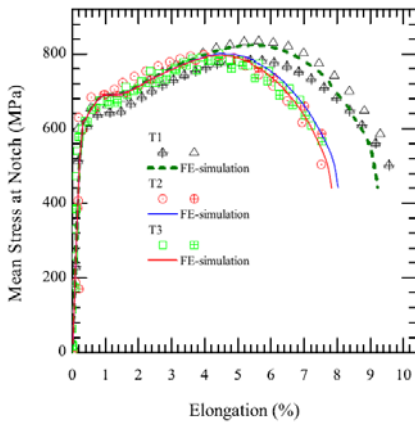


Figure 5: Comparison between the experimental and computational results of engineering stress vs. elongation for notched specimens T1, T2 and T3.

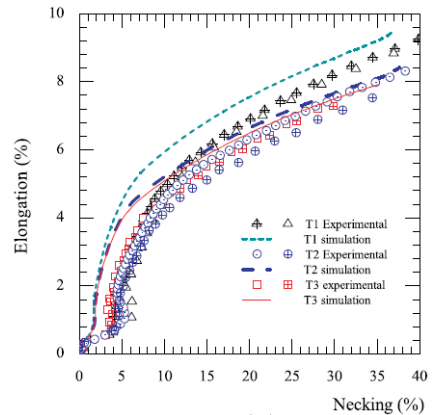


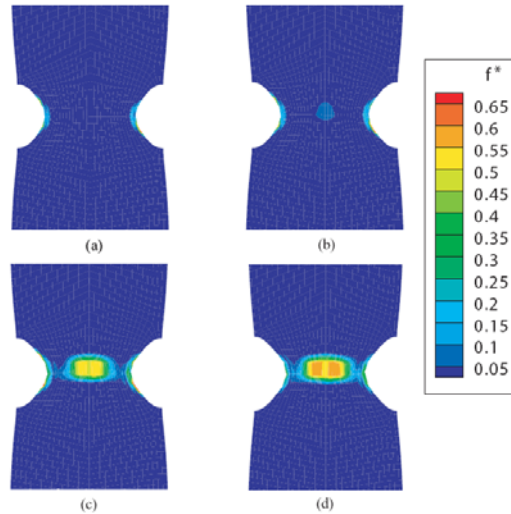
Figure 6: Comparison between the experimental and computational results of necking vs. elongation for notched specimens T1, T2 and T3.

Fig.7 illustrates the contour of the current void volume fraction function  $f^*$  in the area near necking. Different from the results from the smooth tensile specimens, the damage takes place firstly starting from the notched section of the specimen, but it doesn't extend to the center of the specimens from beginning to the end. Finally, the damage takes place in the middle of the specimens just like that of smooth tensile specimens. The computational results of void volume fraction function  $f^*$  increases quickly after  $f_c$ . But the curve from T1 lags that of T2 and T3 much more obviously than that from smooth tensile specimens, which is to say the size effects are much more obvious for notched specimens.

## 6. Conclusions:

The nonlocal damage model modified from the known GTN model is implemented with the element-free Galerkin method into the commercial FEM code ABAQUS. The background FEM cells are treated as elements and the element-free method can be generally realized in the frame of FEM codes.

The computational results are compared with that of experiments for both uniaxial tension specimens and notched specimens and they agree very well. Both experimental and computational results exhibit obvious size effects for the notched specimens in which the smaller ones can afford larger stress and damage more difficultly. The computational accuracy and robustness are higher than the FEM developed based on the  $C^1$  element formulation. The EFG can be used for computational analysis of cracked specimens. The efficiency of the EFG is lower than the corresponding FEM. Results presented in the present paper confirm that the nonlocal damage model with element-free Galerkin method is suitable for computing the damage problems and predicting the size effects.



**Figure 7:** The contour of  $f^*$  in the notched tension specimen T3. (a) The elongation is 7.2%. (b) The elongation is 7.4%. (c) The elongation is 7.6%. (d) The elongation is 8.0%.

## References

- [1] E. C. Aifantis. The physics of plastic deformation. *Int J Plasticity*, 1987, **3**: 211-247
- [2] J. B. Leblond, G. Perrin, J. Devaux. Bifurcation effects in ductile materials with damage localization. *J App Mech* 1994, **61**:236-241
- [3] A. L. Gurson. Continuum theory of ductile rupture by void nucleation and growth: Part I - yield criteria and flow rules for porous ductile media. *J Eng Mat Techn.* 1977, **99**:2-15
- [4] V. Tvergaard, A. Needleman. Analysis of the cup-cone fracture in a round tensile bar. *Acta Metallurgica* 1984, **32**:157-169
- [5] S. Ramasamy, N. Aravas. Finite element implementation of gradient plasticity models Part I and Part II. *Comput Meth Appl Mech Eng* 1998, 163:33-53
- [6] L. P. Mikkelsen, V. Tvergaard. A nonlocal two-dimensional analysis of instabilities in tubes under internal pressure. *J Mech Phys Solids* 1999, 47:953-969
- [7] H. Yuan, J. Chen, K. Krompholz, F. H. Wittmann. Investigations of size effects in tensile tests based on a nonlocal micro-mechanical damage model. *Comp Mat Sci* 2003, **26**:230-243
- [8] W. K. Liu, S. Sun, Y. F. Zhang. Reproducing kernel particle methods. *Int. J. Numer. Methods Eng.* 1995, **20**:1081-1106

- [9] N. Sukumar, B. Moran, T. Black, T. Belytschko. An element-free Galerkin method for three-dimensional fracture mechanics. *Comp Mech* 1997, **20**:170-175
- [10] Y. Xu, S. Saigal. Element free Galerkin study of steady quasi-static crack growth in plane strain tension in elastic-plastic materials. *Comp Mech* 1998, **22**:255-265
- [11] X F Pan, X. Zhang and M W Lu. Meshless Galerkin least-square method. *Comp Mech* 2005, **35**:182-189
- [12] J. Pamin, H. Askes and R. de Borst. Two gradient plasticity theories discretized with the element-free Galerkin method. *Comp Meth in Appl Mech Engng* 2003, **192**, 2377–2403
- [13] H. Askes, E. C. Aifantis. Numerical modeling of size effects with gradient elasticity formulation, meshless discretization and examples. *Int J Fract* 2002, **117**:347---358
- [14] X.-F. Pan, H. Yuan. Application of meshless methods for damage computations with finite strains. Submitted for publication
- [15] X.-F. Pan, H. Yuan. Meshless Method Approaching for strain-gradient based nonlocal damage models in the frame of finite strains. To be submitted for publication